Nesprin-3 regulates endothelial cell morphology, perinuclear cytoskeletal architecture, and flow-induced polarization

Joshua T. Morgan[a], Emily R. Pfeiffer[a], Twanda L. Thirkill[b], Priyadarsini Kumar[b], Gordon Peng[a], Heidi N. Fridolfsson[c], Gordon C. Douglas[b], Daniel A. Starr[c], and Abdul I. Barakat[a,d]

[a]Department of Mechanical and Aerospace Engineering, [b]Department of Cell Biology and Human Anatomy, and [c]Department of Molecular and Cellular Biology, University of California, Davis, Davis, CA 95616; [d]Hydrodynamics Laboratory, Centre National de la Recherche Scientifique (UMR 7646), École Polytechnique, 91128 Palaiseau, France

ABSTRACT Changes in blood flow regulate gene expression and protein synthesis in vascular endothelial cells, and this regulation is involved in the development of atherosclerosis. How mechanical stimuli are transmitted from the endothelial luminal surface to the nucleus is incompletely understood. The linker of nucleus and cytoskeleton (LINC) complexes have been proposed as part of a continuous physical link between the plasma membrane and subnuclear structures. LINC proteins nesprin-1, -2, and -4 have been shown to mediate nuclear positioning via microtubule motors and actin. Although nesprin-3 connects intermediate filaments to the nucleus, no functional consequences of nesprin-3 mutations on cellular processes have been described. Here we show that nesprin-3 is robustly expressed in human aortic endothelial cells (HAECs) and localizes to the nuclear envelope. Nesprin-3 regulates HAEC morphology, with nesprin-3 knockdown inducing prominent cellular elongation. Nesprin-3 also organizes perinuclear cytoskeletal organization and is required to attach the centrosome to the nuclear envelope. Finally, nesprin-3 is required for flow-induced polarization of the centrosome and flow-induced migration in HAECs. These results represent the most complete description to date of nesprin-3 function and suggest that nesprin-3 regulates vascular endothelial cell shape, perinuclear cytoskeletal architecture, and important aspects of flow-mediated mechanotransduction.

INTRODUCTION

The responsiveness of the endothelium—the cellular monolayer lining the inner surfaces of blood vessels—to blood flow–derived mechanical forces regulates normal vascular function and plays a role in the development of atherosclerosis. Although numerous flow-activated biochemical pathways have been described in endothelial cells (ECs; Davies, 1995; Chien, 2007), there is mounting evidence

that mechanical forces at the EC surface are also transmitted to the intracellular space directly via the cytoskeleton (Davies, 1995; Na et al., 2008; Wang et al., 2009). Within this "biophysical" signaling construct, the cytoskeleton plays the role of "hard wiring" ECs and of providing direct physical links between structures at the EC surface and intracellular transduction sites, including the nucleus. We hypothesize that components of recently described protein complexes, the linker of nucleus and cytoskeleton (LINC) complexes (Crisp et al., 2006), play an important role in regulating biophysically mediated mechanotransduction in ECs.

The LINC complexes are conserved from yeast to mammals and function to bridge the nuclear envelope, connecting the cytoskeleton to the nucleoskeleton (Starr, 2009; Starr and Fridolfsson, 2010). The primary components of the LINC complexes are the SUN (Sad1 and UNC-84) proteins in the inner nuclear membrane (INM) that interact with the nucleoskeleton and KASH (Klarsicht, ANC-1, Syne Homology) proteins in the outer nuclear membrane (ONM) that interact directly with the cytoskeleton. KASH and SUN domains

physically interact in the perinuclear space to bridge the nuclear envelope and provide physical continuity between the nuclear and cytoplasmic compartments (Crisp *et al.*, 2006; McGee *et al.*, 2006; Padmakumar *et al.*, 2004). Disruption of this continuity via genetic mutations or deletions in vivo has been linked to muscular, reproductive, and neurological disorders (Grady *et al.*, 2005; Gros-Louis *et al.*, 2007; Wheeler *et al.*, 2007; Zhang *et al.*, 2007a, 2009; Puckelwartz *et al.*, 2009, 2010). Spurred by the apparent functional importance of the LINC complex, there has been a recent surge in research aimed at elucidating the assembly of this complex and the function of its constituents (Razafsky and Hodzic, 2009; Starr, 2009; Starr and Fridolfsson, 2010; Dahl *et al.*, 2010).

The notion of mechanical continuity from the cytoskeleton to the nucleus preceded the canonical description of the LINC complex by several years. Maniotis and colleagues demonstrated that nuclear deformation could be triggered by forces applied to the cell surface and that the deformation was modulated by the cytoskeleton (Maniotis *et al.*, 1997). This work was followed by a study that demonstrated deformation of nucleoli under physiologically relevant loads applied to distant portions of the cell (Hu *et al.*, 2005). Thus it should come as no surprise that there is much speculation about the role of mechanical continuity between the cytoskeleton and the nucleus in mechanotransduction (Mazzag *et al.*, 2003; Gieni and Hendzel, 2008; Wang *et al.*, 2009; Dahl *et al.*, 2010).

There are five known mammalian genes encoding KASH domains. Two of these, *nesp4* (Roux *et al.*, 2009) and *lrmp*, are highly specialized and are respectively expressed only in secretory epithelial cells and lymphocytes; therefore they will not be discussed further. The genes *syne1* and *syne2* encode for multiple isoforms of both nesprin-1 (also called Syne-1, Myne-1, and Enaptin) and nesprin-2 (also called Syne-2 and NUANCE; Apel *et al.*, 2000; Zhang *et al.*, 2001; Zhen *et al.*, 2002; Padmakumar *et al.*, 2004). Nesprin-1 and -2 are very similar, both having giant isoforms (~1000 and ~800 kDa, respectively), long regions containing spectrin repeats, and functional N-terminal actin-binding domains (Padmakumar *et al.*, 2004). Complicating matters are the numerous smaller isoforms of both proteins, with and without KASH domains. In addition, isoforms have been observed at both the INM and ONM, challenging the canonical presentation of the LINC complex (Libotte *et al.*, 2005). Despite these issues, functional roles have been demonstrated for nesprin-1 and -2 in nuclear anchoring (Grady *et al.*, 2005; Zhang *et al.*, 2007b, 2010) and nuclear migration (Zhang *et al.*, 2009). More recently, dominant-negative nesprin constructs and nesprin-1 RNA interference have been shown to interfere with the mechanoresponse of cells to cyclical stretch (Brosig *et al.*, 2010; Chancellor *et al.*, 2010), and nesprin-2 has been implicated in Wnt signaling (Neumann *et al.*, 2010). The final gene encodes nesprin-3α and -3β (Wilhelmsen *et al.*, 2005). Nesprin-3α (referred to as nesprin-3 henceforth), the focus of the current study, differs from nesprin-1 and -2 giants in two key ways: it is smaller (~110 kDa), and its N-terminus has a plectin-binding domain instead of the actin-binding domain found on nesprin-1 and -2. Strong evidence exists that nesprin-3 interacts with intermediate filaments through plectin both in vitro and in vivo (Wilhelmsen *et al.*, 2005; Ketema *et al.*, 2007; Postel *et al.*, 2011). However, no functional role has been demonstrated for nesprin-3. In the present study, we examined the expression, topography, and function of nesprin-3 in human aortic ECs (HAECs).

RESULTS

Nesprin-3 expression and topography in HAECs

We began our investigation of nesprin-3 in human endothelium by verifying the expression and localization of the protein in HAECs in vitro. At the transcript level, RT-PCR revealed a single amplicon of the predicted size for nesprin-3 (Figure 1A). No bands were detected when reverse transcriptase was omitted, confirming that the bands were not the result of contamination with genomic DNA. To study the nesprin-3 protein, a polyclonal antibody against the bulk of the cytoplasmic domain but missing the plectin-interacting domain was raised in rabbits. Verification of protein size via Western blotting produced a single band at ~110 kDa (Figure 1E), corresponding to nesprin-3α. We also observed an inconsistent band at 97 kDa (not shown), which could be a degradation product or a smaller splice variant (nesprin-3β) (Wilhelmsen *et al.*, 2005). Previous studies demonstrated strong localization of nesprin-3 to the nucleus and enrichment at the nuclear periphery in keratinocytes, NIH3T3, and murine embryonic fibroblast cells (Wilhelmsen *et al.*, 2005; Ketema *et al.*, 2007; Postel *et al.*, 2011). Immunofluorescence staining showed that this was also the case for cultured HAECs (Figure 1B).

To verify nesprin-3 expression and localization in vivo, we stained sections of human aortic tissue for nesprin-3 and demonstrated that the protein is indeed expressed in aortic ECs and that, similar to the in vitro case, it exhibits strong nuclear localization (Figure 1C). Confocal analysis on cultured HAECs demonstrated no polarization in nesprin-3's nuclear localization toward either the cell apical or basal surfaces, suggesting uniform coverage of the nuclear envelope (Figure 1D). Silencing nesprin-3 (siN3) achieves specific and near complete knockdown of the protein and transcript 96 h posttransfection as demonstrated using Western blotting, RT-PCR, and immunofluorescence staining (Figure 1, E–G). The recovery of nesprin-3 expression occurs between 120 and 168 h posttransfection (Figure 1, E and G). In addition, although we used small interfering RNA (siRNA) sequences that were not homologous with nesprin-1 and -2, we wanted to confirm that there was no substantial effect of nesprin-3 silencing on their expression. To this end, we confirmed nesprin-1 and -2 transcript presence in both siN3 and control (siNT) HAECs using RT-PCR (Figure 1F).

Stability of nesprin-3 expression and localization under flow

Endothelial cells in vivo are continuously exposed to hemodynamic shear stress, which regulates the expression levels of many proteins, as well as cellular cytoskeletal organization (Davies, 1995). Therefore we asked whether nesprin-3 expression and/or localization were sensitive to flow. To this end, we exposed cultured HAECs in a parallel-plate flow chamber to a steady shear stress at a physiologically relevant level of 15 dyn/cm^2 for periods of either 6 or 24 h. Nesprin-3 staining at the end of the flow period revealed that both the expression (Figure 2A) and localization (Figure 2B) of the protein were insensitive to flow. The same results were observed at other time points (2, 3, 12, and 48 h), different shear stress levels (40 dyn/cm^2), and different flow waveforms (oscillatory flow with an oscillation frequency of 1 Hz) (not shown). These results suggest that nesprin-3 expression and localization are not significantly altered by shear stress.

Effect of nesprin-3 silencing on HAEC morphology

Silencing nesprin-3 in HAECs elicits a striking change in cellular morphology, from the cuboidal shape typical of ECs in static culture (and seen in cells treated with a nontargeting siRNA) to a highly elongated morphology (Figure 3A). The elongation occurs without specific directionality, which is not surprising, given the absence of a directional stimulus, although local groups of cells do exhibit some orientational coordination. HAEC morphology rapidly returns to cuboidal as nesprin-3 expression returns (Figures 1G and 3A), providing further evidence that the morphological response is indeed linked to nesprin-3 expression.
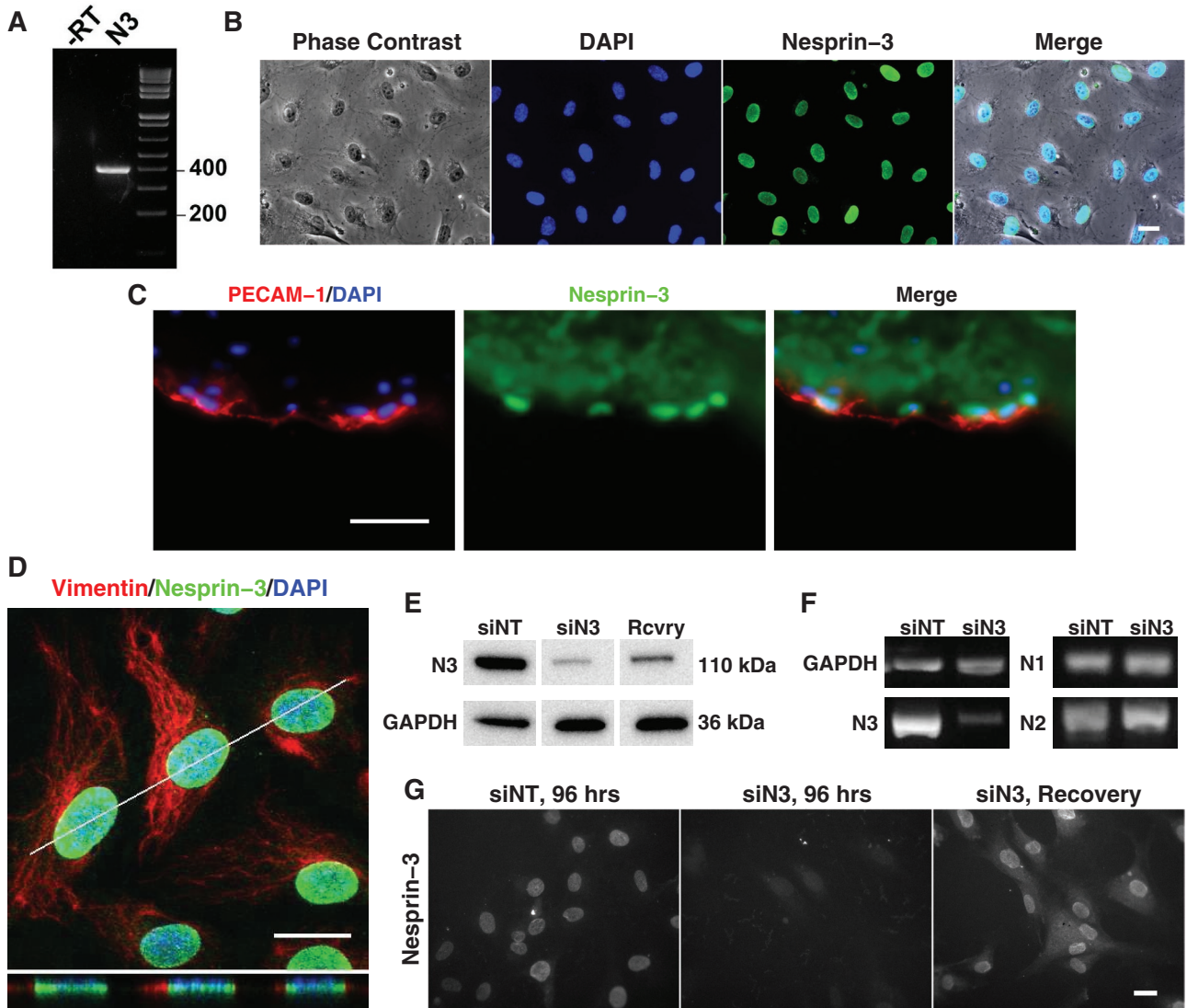
FIGURE 1: Nesprin-3 expression and localization in HAECs. (A) Whole-cell lysates from confluent HAECs were analyzed by RT-PCR for evidence of nesprin-3 (N3) at the transcript level, yielding a single amplicon of the predicted size. When the reverse transcriptase was omitted (–RT), no amplicon was detected. (B) Nesprin-3 localization in cultured HAECs. Bar, 20 µm. (C) Immunofluorescence of nesprin-3 (green) in human aortic sections. The sample is counterstained with PECAM (red) to identify ECs and DAPI (blue) to identify nuclei. Bar, 20 µm. (D) Confocal microscope image of nesprin-3 localization in cultured HAECs. Bottom, a vertical cross section along the white line. DAPI (blue) and anti-vimentin (red) indicate nuclear and cellular extents, respectively. Bar, 20 µm. (E) Western blots against nesprin-3 (top) or GAPDH (bottom) in nontargeting siRNA control cells (siNT), nesprin-3 siRNA cells (siN3) at 96 h posttransfection, and nesprin-3 siRNA cells after recovery (Rcvry). Unrelated bands are trimmed for space. (F) Whole-cell lysates from confluent HAECs were analyzed by RT-PCR for expression of nesprin-1, -2, and -3. GAPDH is included as a loading control. With siN3, there is a loss of nesprin-3, indicating knockdown at the transcript level. This is specific to nesprin-3, as nesprin-1 and -2 show no change in transcript level with siN3 treatment. (G) Immunofluorescence of nesprin-3 in control cells (siNT) or siN3 cells at 96 h posttransfection and after recovery. Bar, 20 µm.

To quantify the observed cellular elongation, we determined the effect of nesprin-3 silencing on HAEC shape index (SI), a dimensionless measure of cell roundness (defined in *Materials and Methods*). Furthermore, as integrin signaling alters cellular cytoskeletal regulation (Huveneers and Danen, 2009), and as integrin activation can depend on extracellular matrix (ECM) composition (Hynes, 2002), we quantified the extent of siN3-mediated elongation for HAECs cultured on uncoated tissue culture plastic (TCP) as well as on TCP coated with collagen, fibronectin, vitronectin, laminin, or bovine serum albumin (BSA). The results demonstrated that nesprin-3 silencing very significantly reduces HAEC SI ($p < 0.0001$). This effect was

virtually identical for all surfaces (Figure 3B), suggesting that integrin-mediated outside-in signaling does not play a major role in the siN3-induced morphological change.

Effect of nesprin-3 silencing on perinuclear cytoskeletal organization in HAECs

In light of the fact that other KASH proteins couple the cytoskeleton to the nuclear envelope, we examined the extent to which nesprin-3 silencing elicits changes in perinuclear cytoskeletal architecture. Because nesprin-3 is known to interact with plectin and to recruit it to the nuclear envelope (Wilhelmsen *et al.*, 2005), we investigated the
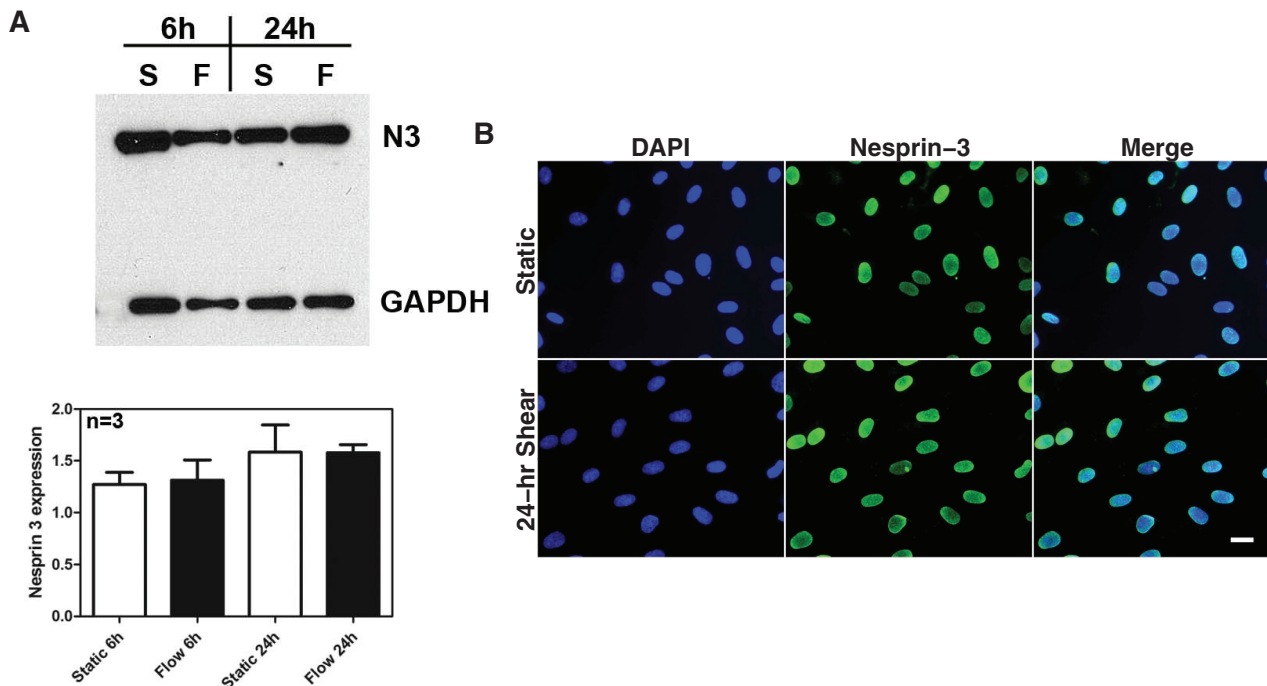
FIGURE 2: Nesprin-3 expression and localization in HAECs are insensitive to fluid dynamic shear stress. (A) Western blot from confluent HAECs under static conditions (S) or 15 dyn/cm² steady shear stress (F) applied for 6 or 24 h. GAPDH is used as an internal control. Quantification of nesprin-3 expression levels is shown below the blot. Data are mean ± SEM (n = 3). (B) Nesprin-3 localization in HAECs is not altered by shear stress at either 6 (not shown) or 24 h. Bar, 20 μm.
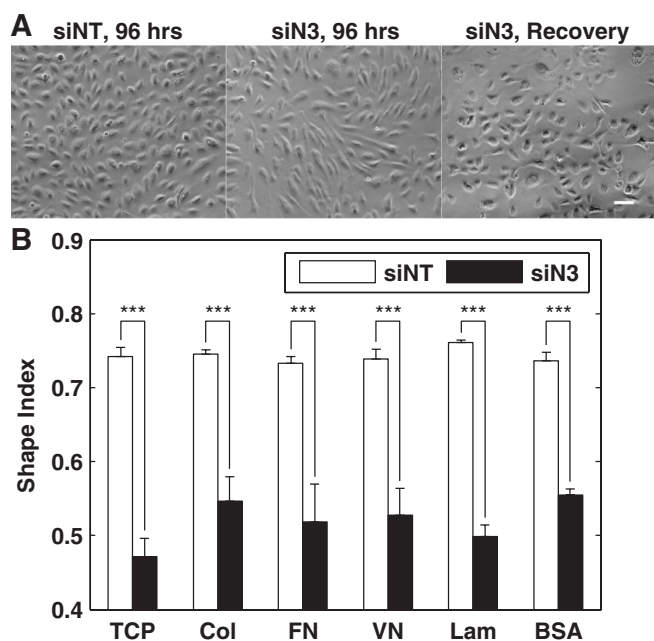

FIGURE 3: Nesprin-3 knockdown leads to elongation of HAECs. (A) Phase contrast images of a field of HAECs treated with nontargeting control siRNA (siNT) or siRNA-mediated knockdown of nesprin-3 (siN3) at 96 h or after recovery. Bar, 80 μm. (B) Quantification of the SI of siN3 and siNT cells (SI = 1 for a circle and SI = 0 for a line). The extent of cell elongation is similar for HAECs plated on tissue culture plastic (TCP), tissue culture plastic coated with collagen (Col), fibronectin (FN), vitronectin (VN), laminin (Lam), or bovine serum albumin (BSA). Data are mean ± SEM (n = 3). ***p < 0.0001 (Tukey's post hoc).

effect of siN3 on plectin. Although plectin distribution in control HAECs exhibited considerable variability, siN3 elicited a clear reduction in plectin staining around the nucleus (Figure 4A), consistent with previous reports (Wilhelmsen *et al.*, 2005; Ketema *et al.*, 2007; Postel *et al.*, 2011). Because plectin may provide a bridge between nesprin-3 and the intermediate filament cytoskeleton as suggested by Wilhelmsen and colleagues, we investigated the effects of siN3 on the localization of vimentin, a major constituent of intermediate filaments in HAECs. The gross morphology of vimentin was not affected by siN3; however, we observed a significant reduction in vimentin localization near the nucleus, resulting in the loss of the intense perinuclear staining present in control cells (Figure 4B).

We quantified the siN3-induced reduction in cytoskeletal staining around the nucleus using two methods. First, we examined the average staining intensity over the nucleus (Figure 4C). Second, we compared the intensity of staining at the nuclear edge to that immediately adjacent, which provides a sense of the brightness of the perinuclear rings observed in control cells (Figure 4D). Both methods revealed significant differences between siN3 and control HAECs, suggesting that nesprin-3 is required for maintenance of perinuclear cytoskeletal architecture. Nesprin-3 silencing had no apparent effect on the gross morphology of the actin and microtubule cytoskeletons, nor was there an apparent effect on flow-induced cytoskeletal remodeling (Supplemental Figure S1).

In addition to its potential role in connecting nesprin-3 to intermediate filaments, plectin, along with its binding partner BRCA2, has been shown to regulate the distance between the microtubule-organizing center (MTOC) and the nucleus (Niwa *et al.*, 2009). Because of the effect that nesprin-3 silencing has on perinuclear plectin organization, we examined whether the distance between the MTOC and the nucleus was altered in siN3
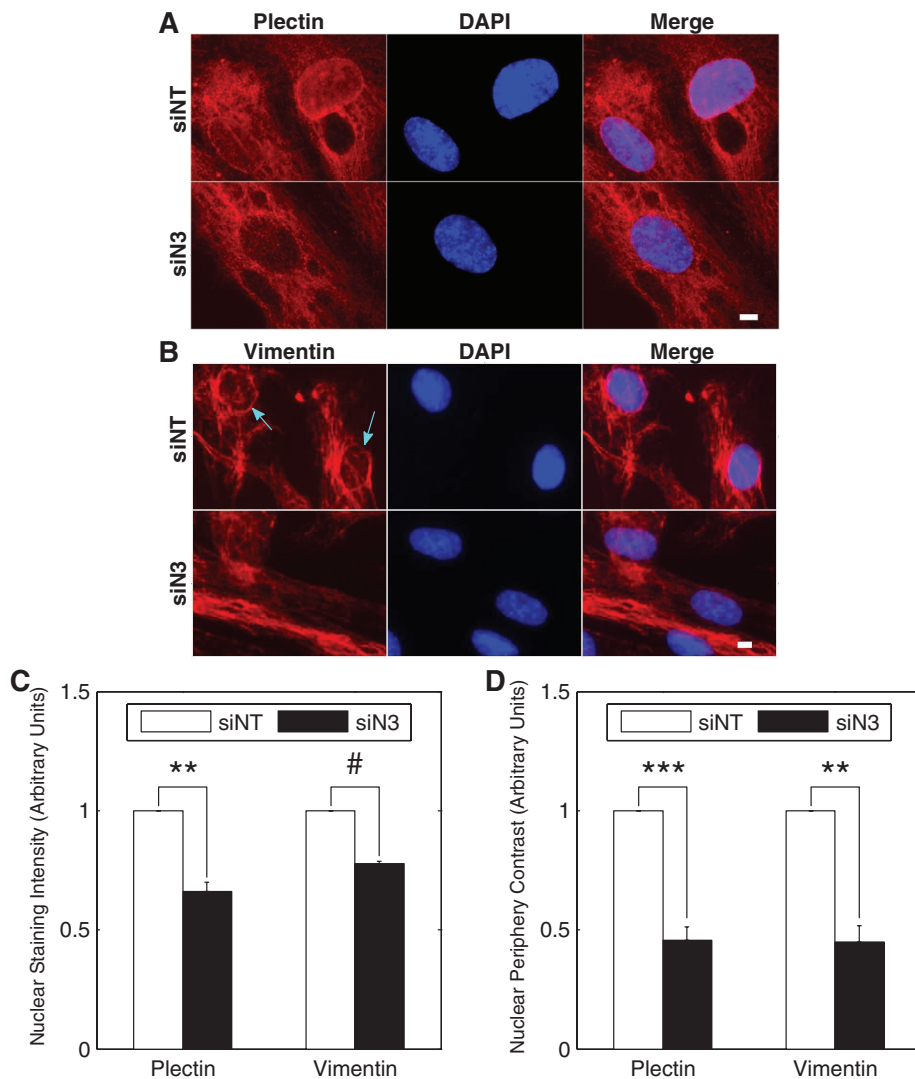
FIGURE 4: Nesprin-3 regulates perinuclear plectin and vimentin architecture in HAECs. (A) Prominent plectin staining over the nucleus and at its periphery present in control (siNT) HAECs is absent following nesprin-3 silencing (siN3). Bar, 5 μm. (B) Vimentin staining in control (siNT) and nesprin-3 knockdown (siN3) HAECs. Prominent perinuclear rings (blue arrows) were only observed in the control cells. Bar, 5 μm. (C, D) Quantification of plectin and vimentin staining intensity over the nucleus and at the nuclear periphery, respectively. In the case of vimentin nuclear staining, data did not display significance using ANOVA against all three controls but did display t test significance against siNT control. Data are mean ± SEM (n = 4 for plectin and n = 3 for vimentin). ***p < 0.0001 (Tukey's post hoc); **p < 0.002 (Tukey's post hoc); #p < 0.025 (paired t test).

HAECs. The results demonstrated that nesprin-3 silencing significantly increases the spacing between the MTOC (demarcated by γ-tubulin staining) and the nucleus (Figure 5). More specifically, the average distance between the MTOC and the nearest nuclear edge was 2.09 ± 0.10 μm (mean ± SEM) in siN3 HAECs vs. 1.42 ± 0.08 μm in control cells (p < 0.002; Figure 5B). This effect is also reflected in a shift in the MTOC–nuclear distance distribution toward larger values, with a large increase in the incidence of cells exhibiting extreme MTOC positions (>3 μm from the nearest nuclear edge) and a concomitant decrease in the incidence of MTOCs positioned adjacent to the nucleus (<1 μm) (Figure 5C). These results suggest that nesprin-3 plays an important role in providing nuclear–MTOC connectivity and that loss of nesprin-3 compromises this connectivity.

Confirmation of static phenotypes using alternate siRNA

To confirm that the cytoskeletal and morphological phenotypes described were not a nonspecific effect of the siRNA, we used a separate set of siRNA targeting nespin-3 (siN3q; Supplemental Figure S2). Although we did achieve substantial knockdown with siN3q treatment, there was noticeably more residual nesprin-3 expression in the HAECs (Supplemental Figure S2, A and B). Although the siN3q HAECs exhibited significant elongation (Supplemental Figure S2C), the effect was not as dramatic as with the more efficient siN3. The perinuclear cytoskeletal disruptions described earlier (nuclear–MTOC distance, loss of plectin and vimentin staining) were also observed with the siN3q HAECs (Supplemental Figure S2, D–F).

Effect of nesprin-3 silencing on flow-induced MTOC polarization and migration

The fact that nesprin-3 regulates nuclear–MTOC connectivity led us to question whether it also regulates MTOC polarization in response to flow. The mechanisms of flow-induced MTOC polarization in ECs remain unclear. In vivo, the magnitude and directionality of this polarization appear to depend on age, species, and the vascular bed studied (Rogers and Kalnins, 1983; Rogers et al., 1985; McCue et al., 2006). In vitro, flow has been shown to elicit sustained MTOC polarization upstream of the nucleus (Vartanian et al., 2008), transient polarization upstream of the nucleus (Galbraith et al., 1998), or sustained polarization downstream of the nucleus (Tzima et al., 2003; McCue et al., 2006). In our HAECs, a steady shear stress of 15 dyn/cm² applied for periods of 2 or 24 h consistently induced MTOC polarization upstream of the nuclear centroid (Figure 6A). Nesprin-3 silencing abolished this polarization, suggesting that nesprin-3 regulates the relative movement of the MTOC and nucleus in response to flow.

Because it has long been known that a relation exists between MTOC polarization and directional cell migration (Malech et al., 1977) and that ECs exposed to flow preferentially migrate downstream (Ando et al., 1987; Masuda and Fujiwara, 1993; Gojova and Barakat, 2005), we suspected that nesprin-3 silencing might also influence HAEC migration in response to flow. As shown in Figure 6B (and time-lapse Supplementary Video S1), control cells exposed to a steady shear stress of 20 dyn/cm² migrate quickly and uniformly in the direction of flow. This is demonstrated by both an increase in cell migration velocity parallel to flow and a reduced angular deviation from the flow when compared with static cells, which display no net directional velocity and a 90° average angle of travel, both indicative of random walk behavior. Nesprin-3
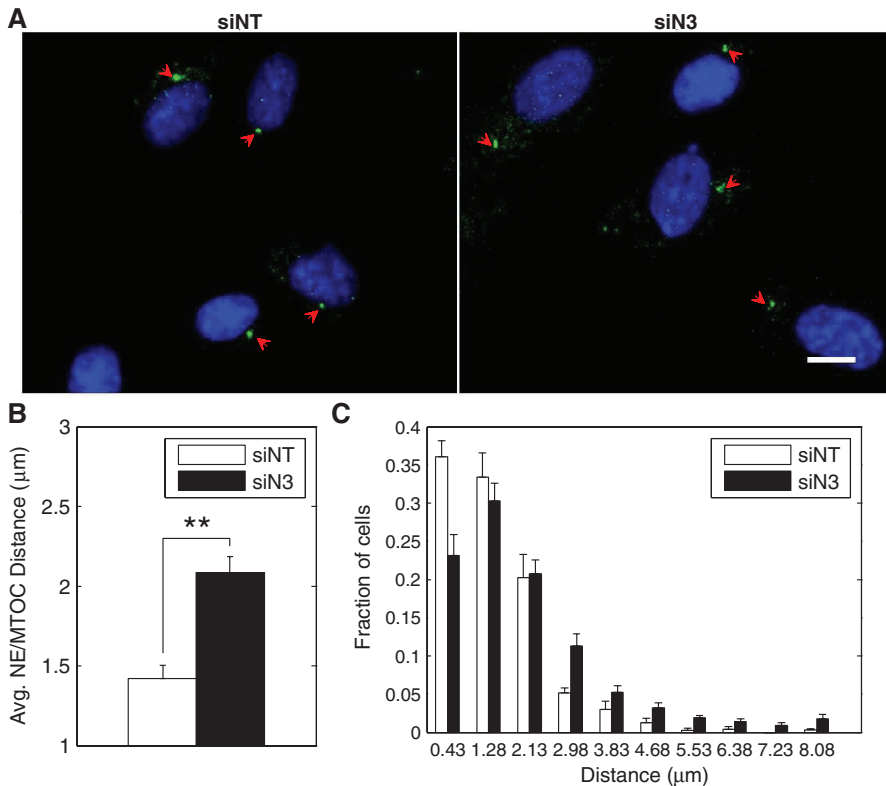
FIGURE 5: Nesprin-3 regulates MTOC–nuclear distance in HAECs. (A) The MTOC, labeled with anti–γ-tubulin (green, marked with red arrowheads), associates with the nucleus (DAPI stained in blue) in control (siNT) HAECs. Following nesprin-3 silencing (siN3), the MTOC is farther from the nucleus. Bar, 10 μm. (B) Average distance between the nuclear envelope and the MTOC increases significantly with nesprin-3 silencing. Data are mean ± SEM (n = 4); **p < 0.002 (Tukey's post hoc). (C) Histogram of the distance between the edge of the nucleus and the MTOC.

uniaxial strain (Chien, 2007), biochemical stimuli such as exposure to vascular endothelial growth factor (Cao et al., 1998), or mechanical constraints, including microchannels or nanoscale surface patterning (Gray et al., 2002; Westwood et al., 2008; Liliensiek et al., 2010). To our knowledge, the present study provides the first example of cellular elongation without external stimulus or constraint, and we are investigating the underlying mechanisms. The fact that such dramatic changes in cellular morphology occur in response to the altered expression of a single protein points to a potentially profound role for nesprin-3 in EC homeostasis.

Previous studies demonstrated that cell shape might be more than a passive indicator of stimulus but also a direct regulator of various cellular functions, including proliferation, apoptosis, and inflammation (Chen et al., 1997, 2003; Vartanian et al., 2010). Therefore the functional ramifications of nesprin-3–mediated morphological changes in ECs merit further investigation. In vivo, ECs in arterial regions prone to the development of atherosclerosis exhibit a cuboidal morphology, whereas cells in zones that are largely protected from atherosclerosis are highly elongated, similar to the siN3 phenotype observed in the present work. Because atherosclerosis is fundamentally an inflammatory disease, an interesting area to explore is the possible role

silencing greatly attenuated the migratory flow response, with the cells moving significantly more slowly in the direction of flow. Although we could partially attribute the lower parallel migration rates to a siN3-mediated reduction in overall cell speed (Supplemental Figure S3), this is also accompanied by a significant increase in angular deviation from purely parallel migration (Figure 6B), indicating a loss of the directional mechanoresponse.

DISCUSSION

In this study, we demonstrated robust expression and nuclear localization of nesprin-3 in human aortic endothelium both in vivo and in vitro. We also demonstrated near-complete and reversible siRNA-mediated nesprin-3 expression knockdown in HAECs. Although nesprin-3 expression was previously demonstrated in a number of tissues (Wilhelmsen et al., 2005; Postel et al., 2011), the present study is the first to show expression in vascular endothelium. The expression and localization of nesprin-3 are insensitive to physiological levels of fluid mechanical shear stress. The stability of nesprin-3 expression may reflect the importance of this protein for a variety of cellular functions, including intracellular structural (cytoskeletal) organization.

No function for nesprin-3 was previously demonstrated, and recent in vivo data from a nesprin-3–deficient zebrafish model show no gross phenotypes (Postel et al., 2011). We used a siRNA approach to identify nesprin-3 cellular functions. We observed that silencing of nesprin-3 induces a dramatic change in cell shape from cuboidal to highly elongated. ECs are known to elongate in response to mechanical stimuli, including unidirectional shear stress or

that nesprin-3 and its effect on EC morphology play in EC inflammation. It is important to note, however, that we observed strong nesprin-3 expression in normal aortic tissue (where ECs were presumably elongated) and after the application of long-term flow in vitro, indicating that loss of nesprin-3 expression is not a requirement for EC elongation and that cellular elongation does not in itself reduce nesprin-3 expression.

The cytoskeletal portion of our study reveals a key feature of the siN3 phenotype: loss of nesprin-3 alters perinuclear cytoskeletal architecture without causing gross alterations in overall cytoskeletal organization. Consistent with previous research (Wilhelmsen et al., 2005; Ketema et al., 2007; Postel et al., 2011), nesprin-3 silencing elicited a dramatic loss of plectin expression around the nucleus. This was accompanied by two additional effects: the loss of vimentin around the nucleus and an increased separation between the MTOC and the nucleus. We propose that nesprin-3 provides a scaffold for plectin perinuclear organization and that nesprin-3 contributes to the connection between the nucleus and the centrosome. This nesprin-3/plectin/vimentin connection would be largely analogous to the nesprin-3/plectin/keratin connection that has been proposed in other cell lines (Wilhelmsen et al., 2005). It should also be noted that the altered nuclear–MTOC spacing observed in the present study appears to be similar to that reported in lamin-deficient fibroblasts (Lee et al., 2007), emerin-deficient fibroblasts (Salpingidou et al., 2007), nesprin-2–deficient keratinocytes (Schneider et al., 2011), nesprin-1/2– or SUN-deficient neurons (Zhang et al., 2009), and plectin- or BRCA2-deficient HeLa cells (Niwa et al., 2009). Taken together, these data suggest a complex picture of nucleoskeletal and
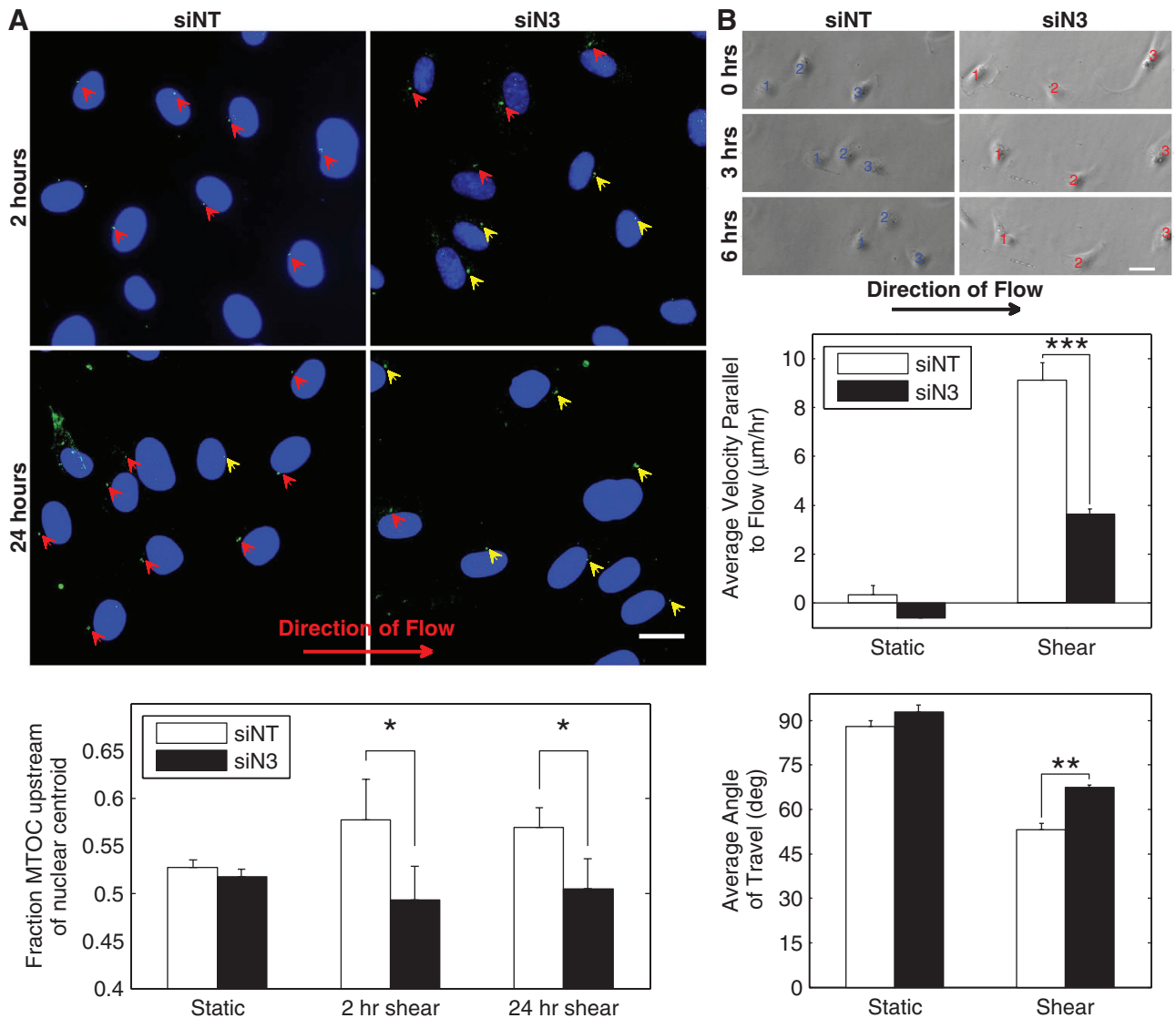
FIGURE 6: Nesprin-3 regulates flow-induced MTOC polarization and migration in HAECs. (A) A steady shear stress of 15 dyn/cm^2 applied for 2 or 24 h elicits MTOC (stained with anti–γ-tubulin in green) polarization upstream of the nuclear centroid in control (siNT) HAECs. Nesprin-3 silencing (siN3) abolishes the effect. The large red arrow denotes the direction of flow, and smaller arrowheads indicate upstream (red) or downstream (yellow) MTOC positions. Bar, 20 μm. Bar graph shows fraction of MTOCs upstream of the nuclear centroid following 2 and 24 h of flow. Data are mean ± SEM (n = 8 for static; n = 5 for 2 h; n = 6 for 24 h). (B) A steady shear stress of 20 dyn/cm^2 elicits highly directional migration of control (siNT) HAECs (blue numbers) parallel to flow. Nesprin-3 silencing (siN3; red numbers) reduces both cell migration velocity and the directionality of migration. Bar, 40 μm. Bar graphs show the average parallel velocity and average angle of travel (n = 4 for static and n = 3 for shear). ***p < 0.0001; **p < 0.005; *p < 0.05 (all by Tukey's post hoc).

cytoskeletal connectivity, with LINC complex proteins providing a critical link between the two skeletal networks.

The importance of nesprin-3 is not necessarily limited to the nuclear envelope, as sequestering plectin and vimentin at the nuclear envelope may affect their availability for other roles. Indeed, recent work shows that plectin/vimentin complexes are important in focal adhesion and shape regulation in mouse fibroblasts (Burgstaller et al., 2010). In addition, in vivo results for both plectin- and vimentin-null mice further highlight the potential importance of the proposed nesprin-3/plectin/vimentin connectivity. Plectin-null mice die shortly after birth due to skin defects (Andra et al., 1997) and exhibit broad phenotypes in mechanically stressed cells. Vimentin-null mice are grossly normal, although they do have a vascular mechanosensitivity phenotype (Henrion et al., 1997). There are many potential

mechanisms for these observations, at least some of which might be related to the nesprin-3 phenotypes we describe here. However, it is difficult to attribute the phenotypes observed in plectin- and vimentin-knockout mice to nesprin-3 because nesprin-3–knockout mice and zebrafish exhibit no apparent gross phenotypes (Starr and Fridolfsson, 2010; Postel et al., 2011). Future work will need to focus on the detailed nature of these connections and their role in modulating cell structure and function.

A key result of the present work is that nesprin-3 expression is required for flow-induced MTOC polarization and directional migration in HAECs. These observations represent the first demonstrations of functional roles for nesprin-3. In light of the fact that MTOC polarization is related to directional mechanoresponse in general (Tzima et al., 2003) and directional migration (Ando et al., 1987) in
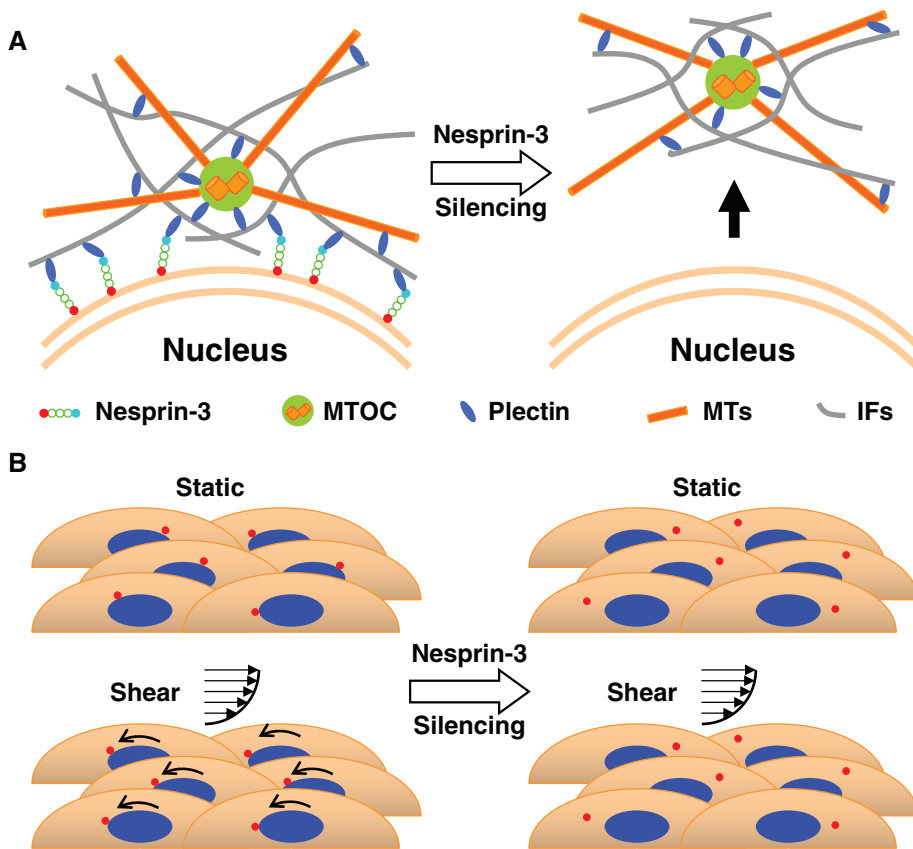
FIGURE 7: Potential model for nesprin-3 modulation of MTOC/nuclear positioning. (A) In a control HAEC, the MTOC is entrapped in the dense perinuclear mesh formed by plectin and intermediate filaments. With the loss of nesprin-3 and the corresponding loss of perinuclear cytoskeleton, the MTOC is free to drift away from the nucleus and interact with the cytoskeleton elsewhere in the cell. (B) This loss of connectivity between the nuclei (blue ellipses) and the MTOCs (red dots) leads to an inability of MTOCs to polarize with the application of flow.

nuclear connectivity potentially inhibits cellular functions such as polarization in response to shear (Figure 7B).

The present results demonstrate that nesprin-3 plays a structural role in ECs by organizing perinuclear cytoskeletal architecture as well as a functional role by modulating flow-induced MTOC polarization and migration. The finding of a role for nesprin-3 in EC responsiveness to flow complements recent data implicating nesprin-1 in stretch-induced cellular reorientation in ECs (Chancellor et al., 2010) and stretch-induced nuclear rotation in fibroblasts (Brosig et al., 2010). Together, these results suggest that the nesprin proteins are important regulators of cellular mechanotransduction, although the underlying mechanisms and signaling pathways remain unknown. One particularly intriguing idea in this context is a role for nesprin in "biophysical" mechanotransduction, by which mechanical forces generated within or relayed to the cytoskeleton are transmitted directly to the nucleus via nesprins and/or other constituents of the LINC complex. There is evidence that disruption of the LINC complex broadly alters cytoskeletal mechanics (Lee et al., 2007; Stewart-Hutchinson et al., 2008), which might in turn affect mechanosensitive molecules throughout the cell. These biophysical signaling modalities, by which mechanics regulates intracellular signaling, promise to provide answers for many of the outstanding questions in cellular mechanobiology.

particular, it is likely that these two phenotypes are linked and point to a potentially broader role for nesprin-3 in EC mechanotransduction. The present study does not inform us whether flow-induced MTOC polarization was abolished due to a loss of downstream motion of the nucleus [similar to the rearward nuclear motion in a migrating fibroblast (Gomes et al., 2005)], a loss of upstream motion of the MTOC, or a combination of the two. Both possibilities are potentially attributable to the loss of nuclear/cytoskeletal connectivity caused by nesprin-3 silencing.

The demonstration of nesprin-3's role in maintaining normal MTOC/nuclear positioning adds to an already complex picture of perinuclear cytoskeletal structure and organization. Speculation from previous studies can be organized into two general categories: either a "passive" positioning mediated by structural protein bridges between the nucleus and the MTOC (Lee et al., 2007; Salpingidou et al., 2007; Niwa et al., 2009; Zhang et al., 2009) or an "active" connection mediated by competitive activity of the molecular motors kinesin and dynein (Roux et al., 2009; Schneider et al., 2011). In conjunction with the previous demonstration of the importance of plectin (Niwa et al., 2009), our results suggest that nesprin-3 may mediate MTOC/nuclear connectivity through plectin and intermediate filaments (Figure 7A). The MTOC becomes entrapped in a dense mesh of perinuclear intermediate filaments via plectin cross-linkers. Without nesprin-3, the perinuclear mesh disappears and the MTOC is free to bind to undisturbed regions of the cytoskeleton, far from the nucleus. Given the importance of the MTOC, the loss of MTOC/

MATERIALS AND METHODS
Cell culture and application of shear
HAECs (passages 4–7; Cascade Biologics, Portland, OR) were plated at subconfluent density on collagen-coated Permanox Lab-Tek Chamber Slides (Nalge Nunc, Rochester, NY) and cultured using standard procedures (Suvatne et al., 2001) in EGM-2 growth media (Lonza, Basel, Switzerland). For the experiments testing the effect of ECM proteins, the procedures were identical but with the slides either uncoated or coated with other ECM proteins as described in *Results*. For the siRNA experiments, cells were transfected using DharmaFECT siRNA Transfection Reagent 4 (Dharmacon, Thermo Fisher Scientific, Waltham, MA) with either nesprin-3-targeting ON-TARGETplus SMARTpool siRNA (L-016637-01-0005) or a nontargeting siRNA (ON-TARGETplus non-targeting siRNA #4; Dharmacon) and incubated in the transfection reagents overnight for 48 h at 37°C and 5% CO_2. Cells were maintained for an additional 48 h in EGM-2, which corresponded to optimum nesprin-3 knockdown. Additional reagent-only (no siRNA) and media-only controls were performed and yielded similar results to the nontargeting siRNA controls. An alternate pool of siRNAs targeting nesprin-3 consisting of four different siRNAs (SI04258205, SI04357542, SI00320124, SI04146562) in equal parts (Qiagen, Valencia, CA) was used to check for nonspecific effects. For the flow experiments, the cells were placed in a parallel-plate flow chamber and exposed using a recirculating flow loop to a steady shear stress of 15 dyn/cm² at 37°C and 5% CO_2 (Suvatne et al., 2001). Migration experiments were conducted as earlier, except that the

cells remained subconfluent to allow for unhindered migration of individual cells, and shear was applied at 20 dyn/cm^2 for ~6 h. A single field was collected every 10 min.

Nesprin-3 antibody

The sequence encoding human nesprin-3 (67–925), including everything except the N-terminal plectin-binding domain and the C-terminal KASH and transmembrane domains, was amplified from the FLJ16564 cDNA (Invitrogen, Carlsbad, CA) with *Mfe*I overhanging restriction sites and cloned into the *Eco*RI site of pGEX-2T (GE Healthcare, Little Chalfont, United Kingdom) to create pSL132. Glutathione *S*-transferase (GST)–nesprin-3 protein was expressed in *Escherichia coli* strain BL21 codon plus (Stratagene, Santa Clara, CA) and purified on glutathione–Sepharose 4B beads (GE Healthcare). Two rabbits were injected with purified fusion protein with assistance from the Laboratory of Comparative Pathology at the School of Veterinary Medicine, University of California, Davis. Anti–GST-nesprin-3 serum from rabbit 2325 was used in all experiments.

Western blotting

Transfected and control cells were lysed in lysis buffer composed of 1% SDS, 10 mM Tris, 5 mM ethylene glycol tetraacetic acid, 3:100 P8340 Protease Inhibitor Cocktail (Sigma-Aldrich, Saint Louis, MO), and 4 μM sodium orthovanadate in prechilled microcentrifuge tubes. After electrophoresis, proteins were transferred to polyvinylfluoride membrane and primary antibodies were applied overnight. Rabbit anti–nesprin-3 antiserum was used at a 1:5000 dilution and mouse anti–glyceraldehyde-3-phosphate dehydrogenase (GAPDH) antibody at a 1:2500 dilution (Santa Cruz Biotechnology, Santa Cruz, CA). Horseradish peroxidase–conjugated anti–mouse or anti–rabbit secondary antibodies (Pierce, Rockford, IL) were applied at 1:2500 for 1 h. Labeled membranes were incubated with SuperSignal West Dura Substrate (Pierce) for 5 min, exposed to film, developed, and scanned for quantification. Scanned membranes were quantified in SimplePCI (Hamamatsu, Sewickley, PA). Protein band intensity was measured and normalized to GAPDH.

Immunohistochemistry

Cryosections of human aorta were obtained from ProSci (Poway, CA) and fixed in acetone (prechilled to −20°C). Sections were stained overnight using a rabbit polyclonal nesprin-3 antibody at a 1:100 dilution, and a 1:10 dilution of mouse monoclonal antibody against CD31 (PECAM-1; clone JC70A from DAKO North America, Carpinteria, CA). After washing, the sections were incubated with Alexa Fluor 488–labeled goat anti–rabbit immunoglobulin G (IgG) and Alexa Fluor 594–labeled rabbit anti–mouse IgG. To control for nonspecific staining, primary antibodies were replaced with matched control immunoglobulins. Nuclei were stained by incubating sections with 220 nM 4′,6-diamidino-2-phenylindole (DAPI; Invitrogen) in Tris-buffered saline for 5 min. Sections were mounted in GVA mounting medium (Invitrogen) and examined using an epifluorescence microscope.

Immunofluorescence

For immunofluorescence, cells were washed with warm phosphate-buffered saline containing calcium and magnesium (Invitrogen) and immediately fixed and permeabilized for 5 min in warm PEM buffer with 3.7% formaldehyde (Sigma-Aldrich) and 0.2% Triton X-100 (Sigma-Aldrich). Staining antibodies were as follows: rabbit anti–γ-tubulin (Sigma-Aldrich) for MTOC at a 1:200 dilution, rabbit anti–nesprin-3 antiserum at a 1:400 dilution, goat anti-plectin at a 1:200

dilution (Santa Cruz Biotechnology), and mouse anti-vimentin at a 1:500 dilution (Sigma-Aldrich). After washing, the sections were incubated with Alexa Fluor 488–labeled goat anti–rabbit IgG or Alexa Fluor 555–labeled goat anti–mouse IgG. Nuclei were counterstained using DAPI (Invitrogen). After staining, the cells were mounted in GVA mounting media (Invitrogen) with 0.2 M 1,4-diazabicyclo[2.2.2] octane (Sigma-Aldrich). Cells were imaged on a Nikon TE300 Eclipse inverted microscope (Nikon, Melville, NY) with a 40× Plan Fluor objective (numerical aperture, 0.6) and QCapture Imaging Suite running a Retiga 1300 monochrome camera (Q-Imaging, Surrey, Canada). Confocal images were collected on an Olympus FV1000 confocal microscope (Olympus America, Center Valley, PA).

RT-PCR

Total RNA was isolated from HAECs using TRIzol (Invitrogen) and digested with DNase (Invitrogen). A 2-μl amount of the RNA was denatured at 7°C for 10 min, pulse centrifuged, and chilled on ice. After reverse transcription, the converted-to-cDNA product was used for PCR analysis. Control samples in which the RT step was omitted were also included. Primers to detect nesprin-3 (NM_152592.3) were as follows: forward, CCTGCAGAGGAAAAGCAAAC; reverse, GTGGTCACAACGATCCACTG. The product size was 396 base pairs and was sequenced to confirm identity.

For verification of knockdown specificity, we used 35 PCR cycles, empirically chosen as below the plateau threshold for the nesprins. Primers to detect nesprin-1 (NM_182961.3) were as follows: forward, AGTCTGGAGGCGAAAGTCAA; reverse, CGGTCTTCAAAACCAGCAAT. The product size was 191 base pairs. Primers to detect nesprin-2 (NM_033071.3) were as follows: forward, GCAGGCAGCTGTGGTACAATATGA; reverse, ACCGTCAGCAGCATGGTGGC. The product size was 255 base pairs. Primers to detect GAPDH (NM_002046.3) were as follows: forward, TTCATTGACCTCAACTACAT; reverse, GAGGGGCCATCCACAGTCTT. The product size was 496 base pairs.

Image analysis

For cell morphology analysis, individual cells were hand traced and elongation quantified using the SI, a dimensionless measure of circularity defined as follows: $SI = 4\pi \times area/(perimeter)^2$. Thus $SI = 1$ for a circle and $SI = 0$ for a line. For intensity measurements, background was subtracted using a rolling-ball type filter with a 42.5-μm radius, and each experiment was normalized to the average value of the nontargeting siRNA control. For nuclear intensities, the "nuclear" region was defined using the DAPI stain. For nuclear periphery contrast, staining intensity was averaged over an ~0.5-μm border region enclosing the DAPI stain and compared with the average staining intensity of the two adjacent similar-thickness regions. For MTOC localization, the nuclear region was defined using the DAPI stain, and MTOCs were manually identified using the γ-tubulin stain. Positioning in relation to the nuclear edge and nuclear centroid was scored. For migration analysis, all images from an experiment were assembled into a time-lapse video and individual cells were manually tracked. The velocity of a cell parallel to flow was determined as $V_{parallel} = d_{parallel}/t$, where $d_{parallel}$ denotes the net cell displacement parallel to flow and t is the total time elapsed. This results in zero velocities for a purely random walk, positive values for net migration in the direction of flow, and negative values for net migration against flow. The angle of travel was defined as $\theta = \tan^{-1}(d_{perpendicular}/d_{parallel})$, where $d_{perpendicular}$ denotes the net cell displacement perpendicular to flow. This definition results in an angle of 90° for a random walk, 180° for purely antiparallel

migration, and 0° for purely parallel migration. All image analysis was performed in MATLAB 2007b (Mathworks, Natick, MA).

Statistical analysis

Comparisons were made among the treatment and the three control groups (nontargeting siRNA, reagents only, and media only) using either repeated-measures analysis of variance (ANOVA) (for the polarization study) or one-way ANOVA (for elongation and cytoskeletal work), followed by Tukey's post hoc test. In the case of nuclear vimentin staining, staining variability in the reagent and media controls prevented significance by ANOVA, and lesser significance was achieved using a paired t test between the siN3 group and the nontargeting siRNA control group. Migration data were collected only for the siN3 and the nontargeting siRNA control, and comparisons were made using one-way ANOVA followed by Tukey's post hoc test. All statistical calculations were performed in MATLAB 2007b (Mathworks).

REFERENCES

Ando J, Nomura H, Kamiya A (1987). The effect of fluid shear stress on the migration and proliferation of cultured endothelial cells. Microvasc Res 33, 62–70.

Andra K, Lassmann H, Bittner R, Shorny S, Fassler R, Propst F, Wiche G (1997). Targeted inactivation of plectin reveals essential function in maintaining the integrity of skin, muscle, and heart cytoarchiture. Genes Dev 11, 3143–3156.

Apel ED, Lewis RM, Grady RM, Sanes JR (2000). Syne-1, a dystrophin- and Klarsicht-related protein associated with synaptic nuclei at the neuromuscular junction. J Biol Chem 275, 31986–31995.

Brosig M, Ferralli J, Gelman L, Chiquet M, Chiquet-Ehrismann R (2010). Interfering with the connection between the nucleus and the cytoskeleton affects nuclear rotation, mechanotransduction and myogenesis. Int J Biochem Cell Biol 42, 1717–1728.

Burgstaller G, Gregor M, Winter L, Wiche G (2010). Keeping the vimentin network under control: cell-matrix adhesion-associated plectin 1f affects cell shape and polarity of fibroblasts. Mol Biol Cell 21, 3362–3375.

Cao Y, Linden P, Farnebo J, Cao R, Eriksson A, Kumar V, Qi JH, Claesson-Welsh L, Alitalo K (1998). Vascular endothelial growth factor C induces angiogenesis in vivo. Proc Natl Acad Sci USA 95, 14389–14394.

Chancellor TJ, Lee J, Thodeti CK, Lele T (2010). Actomyosin tension exerted on the nucleus through nesprin-1 connections influences endothelial cell adhesion, migration, and cyclic strain-induced reorientation. Biophys J 99, 115–123.

Chen CS, Alonso JL, Ostuni E, Whitesides GM, Ingber DE (2003). Cell shape provides global control of focal adhesion assembly. Biochem Biophys Res Commun 307, 355–361.

Chen CS, Mrksich M, Huang S, Whitesides GM, Ingber DE (1997). Geometric control of cell life and death. Science 276, 1425–1428.

Chien S (2007). Mechanotransduction and endothelial cell homeostasis: the wisdom of the cell. Am J Physiol 292, H1209–1224.

Crisp M, Liu Q, Roux K, Rattner JB, Shanahan C, Burke B, Stahl PD, Hodzic D (2006). Coupling of the nucleus and cytoplasm: role of the LINC complex. J Cell Biol 172, 41–53.

Dahl KN, Booth-Gauthier EA, Ladoux B (2010). In the middle of it all: mutual mechanical regulation between the nucleus and the cytoskeleton. J Biomech 43, 2–8.

Davies PF (1995). Flow-mediated endothelial mechanotransduction. Physiol Rev 75, 519–560.

Galbraith CG, Skalak R, Chien S (1998). Shear stress induces spatial reorganization of the endothelial cell cytoskeleton. Cell Motil Cytoskeleton 40, 317–330.

Gieni RS, Hendzel MJ (2008). Mechanotransduction from the ECM to the genome: are the pieces now in place? J Cell Biochem 104, 1964–1987.

Gojova A, Barakat AI (2005). Vascular endothelial wound closure under shear stress: role of membrane fluidity and flow-sensitive ion channels. J Appl Physiol 98, 2355–2362.

Gomes ER, Jani S, Gundersen GG (2005). Nuclear movement regulated by Cdc42, MRCK, myosin, and actin flow establishes MTOC polarization in migrating cells. Cell 121, 451–463.

Grady RM, Starr DA, Ackerman GL, Sanes JR, Han M (2005). Syne proteins anchor muscle nuclei at the neuromuscular junction. Proc Natl Acad Sci USA 102, 4359–4364.

Gray BL, Lieu DK, Collins SD, Smith RL, Barakat AI (2002). Microchannel platform for the study of endothelial cell shape and function. Biomed Microdev 4, 9–16.

Gros-Louis F, Dupre N, Dion P, Fox MA, Laurent S, Verreault S, Sanes JR, Bouchard JP, Rouleau GA (2007). Mutations in SYNE1 lead to a newly discovered form of autosomal recessive cerebellar ataxia. Nat Genet 39, 80–85.

Henrion D et al. (1997). Impaired flow-induced dilation in mesenteric resistance arteries from mice lacking vimentin. J Clin Invest 100, 2909–2914.

Hu S, Chen J, Butler JP, Wang N (2005). Prestress mediates force propagation into the nucleus. Biochem Biophys Res Commun 329, 423–428.

Huveneers S, Danen EH (2009). Adhesion signaling—crosstalk between integrins, Src and Rho. J Cell Sci 122, 1059–1069.

Hynes RO (2002). Integrins: bidirectional, allosteric signaling machines. Cell 110, 673–687.

Ketema M, Wilhelmsen K, Kuikman I, Janssen H, Hodzic D, Sonnenberg A (2007). Requirements for the localization of nesprin-3 at the nuclear envelope and its interaction with plectin. J Cell Sci 120, 3384–3394.

Lee JS, Hale CM, Panorchan P, Khatau SB, George JP, Tseng Y, Stewart CL, Hodzic D, Wirtz D (2007). Nuclear lamin A/C deficiency induces defects in cell mechanics, polarization, and migration. Biophys J 93, 2542–2552.

Libotte T et al. (2005). Lamin A/C-dependent localization of Nesprin-2, a giant scaffolder at the nuclear envelope. Mol Biol Cell 16, 3411–3424.

Liliensiek SJ, Wood JA, Yong J, Auerbach R, Nealey PF, Murphy CJ (2010). Modulation of human vascular endothelial cell behaviors by nanotopographic cues. Biomaterials 31, 5418–5426.

Malech HL, Root RK, Gallin JI (1977). Structural analysis of human neutrophil migration. Centriole, microtubule, and microfilament orientation and function during chemotaxis. J Cell Biol 75, 666–693.

Maniotis AJ, Chen CS, Ingber DE (1997). Demonstration of mechanical connections between integrins, cytoskeletal filaments, and nucleoplasm that stabilize nuclear structure. Proc Natl Acad Sci USA 94, 849–854.

Masuda M, Fujiwara K (1993). The biased lamellipodium development and microtubule organizing center position in vascular endothelial cells migrating under the influence of fluid flow. Biol Cell 77, 237–245.

Mazzag BM, Tamaresis JS, Barakat AI (2003). A model for shear stress sensing and transmission in vascular endothelial cells. Biophys J 84, 4087–4101.

McCue S, Dajnowiec D, Xu F, Zhang M, Jackson MR, Langille BL (2006). Shear stress regulates forward and reverse planar cell polarity of vascular endothelium in vivo and in vitro. Circ Res 98, 939–946.

McGee MD, Rillo R, Anderson AS, Starr DA (2006). UNC-83 IS a KASH protein required for nuclear migration and is recruited to the outer nuclear membrane by a physical interaction with the SUN protein UNC-84. Mol Biol Cell 17, 1790–1801.

Na S, Collin O, Chowdhury F, Tay B, Ouyang M, Wang Y, Wang N (2008). Rapid signal transduction in living cells is a unique feature of mechanotransduction. Proc Natl Acad Sci USA 105, 6626–6631.

Neumann S, Schneider M, Daugherty RL, Gottardi CJ, Eming SA, Beijer A, Noegel AA, Karakesisoglou I (2010). Nesprin-2 interacts with alpha-catenin and regulates Wnt signaling at the nuclear envelope. J Biol Chem 285, 34932–34938.

Niwa T, Saito H, Imajoh-ohmi S, Kaminishi M, Seto Y, Miki Y, Nakanishi A (2009). BRCA2 interacts with the cytoskeletal linker protein plectin to form a complex controlling centrosome localization. Cancer Sci 100, 2115–2125.

Padmakumar VC, Abraham S, Braune S, Noegel AA, Tunggal B, Karakesisoglou I, Korenbaum E (2004). Enaptin, a giant actin-binding protein, is an element of the nuclear membrane and the actin cytoskeleton. Exp Cell Res 295, 330–339.

Postel R, Ketema M, Kuikman I, de Pereda JM, Sonnenberg A (2011). Nesprin-3 augments peripheral nuclear localization of intermediate filaments in zebrafish. J Cell Sci 124, 755–764.

Puckelwartz MJ et al. (2009). Disruption of nesprin-1 produces an Emery Dreifuss muscular dystrophy-like phenotype in mice. Hum Mol Genet 18, 607–620.

Puckelwartz MJ et al. (2010). Nesprin-1 mutations in human and murine cardiomyopathy. J Mol Cell Cardiol 48, 600–608.

Razafsky D, Hodzic D (2009). Bringing KASH under the SUN: the many faces of nucleo-cytoskeletal connections. J Cell Biol 186, 461–472.

Rogers KA, Kalnins VI (1983). Comparison of the cytoskeleton in aortic endothelial cells in situ and in vitro. Lab 49, 650–654.

Rogers KA, McKee NH, Kalnins VI (1985). Preferential orientation of centrioles toward the heart in endothelial cells of major blood vessels is reestablished after reversal of a segment. Proc Natl Acad Sci USA 82, 3272–3276.

Roux KJ, Crisp ML, Liu Q, Kim D, Kozlov S, Stewart CL, Burke B (2009). Nesprin 4 is an outer nuclear membrane protein that can induce kinesin-mediated cell polarization. Proc Natl Acad Sci USA 106, 2194–2199.

Salpingidou G, Smertenko A, Hausmanowa-Petrucewicz I, Hussey PJ, Hutchison CJ (2007). A novel role for the nuclear membrane protein emerin in association of the centrosome to the outer nuclear membrane. J Cell Biol 178, 897–904.

Schneider M, Lu W, Neumann S, Brachner A, Gotzmann J, Noegel AA, Karakesisoglou I (2011). Molecular mechanisms of centrosome and cytoskeleton anchorage at the nuclear envelope. Cell Mol Life Sci 68, 1593–1610.

Starr DA (2009). A nuclear-envelope bridge positions nuclei and moves chromosomes. J Cell Sci 122, 577–586.

Starr DA, Fridolfsson HN (2010). Interactions between nuclei and the cytoskeleton are mediated by SUN-KASH nuclear-envelope bridges. Annu Rev Cell Dev Biol 26, 421–444.

Stewart-Hutchinson PJ, Hale CM, Wirtz D, Hodzic D (2008). Structural requirements for the assembly of LINC complexes and their function in cellular mechanical stiffness. Exp Cell Res 314, 1892–1905.

Suvatne J, Barakat AI, O'Donnell ME (2001). Flow-induced expression of endothelial Na-K-Cl cotransport: dependence on K^+ and Cl^- channels. Am J Physiol 280, C216–C227.

Tzima E, Kiosses WB, del Pozo MA, Schwartz MA (2003). Localized cdc42 activation, detected using a novel assay, mediates microtubule organizing center positioning in endothelial cells in response to fluid shear stress. J Biol Chem 278, 31020–31023.

Vartanian KB, Berny MA, McCarty OJ, Hanson SR, Hinds MT (2010). Cytoskeletal structure regulates endothelial cell immunogenicity independent of fluid shear stress. Am J Physiol 298, C333–C341.

Vartanian KB, Kirkpatrick SJ, Hanson SR, Hinds MT (2008). Endothelial cell cytoskeletal alignment independent of fluid shear stress on micropatterned surfaces. Biochem Biophys Res Commun 371, 787–792.

Wang N, Tytell JD, Ingber DE (2009). Mechanotransduction at a distance: mechanically coupling the extracellular matrix with the nucleus. Nat Rev Mol Cell Biol 10, 75–82.

Westwood SM, Gray BL, Grist S, Huffman K, Jaffer S, Kavanagh KL (2008). SU-8 polymer enclosed microchannels with interconnect and nanohole arrays as an optical detection device for biospecies. Proc IEEE Eng Med Biol Soc 2008, 5652–5655.

Wheeler MA, Davies JD, Zhang Q, Emerson LJ, Hunt J, Shanahan CM, Ellis JA (2007). Distinct functional domains in nesprin-1alpha and nesprin-2beta bind directly to emerin and both interactions are disrupted in X-linked Emery-Dreifuss muscular dystrophy. Exp Cell Res 313, 2845–2857.

Wilhelmsen K, Litjens SH, Kuikman I, Tshimbalanga N, Janssen H, van den Bout I, Raymond K, Sonnenberg A (2005). Nesprin-3, a novel outer nuclear membrane protein, associates with the cytoskeletal linker protein plectin. J Cell Biol 171, 799–810.

Zhang J et al. (2010). Nesprin 1 is critical for nuclear positioning and anchorage. Hum Mol Genet 19, 329–341.

Zhang Q et al. (2007a). Nesprin-1 and -2 are involved in the pathogenesis of Emery Dreifuss muscular dystrophy and are critical for nuclear envelope integrity. Hum Mol Genet 16, 2816–2833.

Zhang Q, Skepper JN, Yang F, Davies JD, Hegyi L, Roberts RG, Weissberg PL, Ellis JA, Shanahan CM (2001). Nesprins: a novel family of spectrin-repeat-containing proteins that localize to the nuclear membrane in multiple tissues. J Cell Sci 114, 4485–4498.

Zhang X, Lei K, Yuan X, Wu X, Zhuang Y, Xu T, Xu R, Han M (2009). SUN1/2 and Syne/Nesprin-1/2 complexes connect centrosome to the nucleus during neurogenesis and neuronal migration in mice. Neuron 64, 173–187.

Zhang X, Xu R, Zhu B, Yang X, Ding X, Duan S, Xu T, Zhuang Y, Han M (2007b). Syne-1 and Syne-2 play crucial roles in myonuclear anchorage and motor neuron innervation. Development 134, 901–908.

Zhen YY, Libotte T, Munck M, Noegel AA, Korenbaum E (2002). NUANCE, a giant protein connecting the nucleus and actin cytoskeleton. J Cell Sci 115, 3207–3222.